



**HAL**  
open science

## Comprehensive Study of the Low-Temperature Transport and Thermodynamic Properties of the Cluster Compounds $\text{Ag}_x\text{Mo}_9\text{Se}_{11}$ ( $3.41 \leq x \leq 3.78$ )

Tong Zhou, Malika Colin, Christophe Candolfi, Clotilde Boulanger, Anne Dauscher, Eva Šantavá, Jiří Hejtmánek, Philippe Baranek, Rabih Al Rahal Al Orabi, Michel Potel, et al.

### ► To cite this version:

Tong Zhou, Malika Colin, Christophe Candolfi, Clotilde Boulanger, Anne Dauscher, et al.. Comprehensive Study of the Low-Temperature Transport and Thermodynamic Properties of the Cluster Compounds  $\text{Ag}_x\text{Mo}_9\text{Se}_{11}$  ( $3.41 \leq x \leq 3.78$ ). *Chemistry of Materials*, 2014, 26 (16), pp.4765-4775. 10.1021/cm5016367 . hal-01088532

**HAL Id: hal-01088532**

**<https://hal.science/hal-01088532>**

Submitted on 6 Apr 2023

**HAL** is a multi-disciplinary open access archive for the deposit and dissemination of scientific research documents, whether they are published or not. The documents may come from teaching and research institutions in France or abroad, or from public or private research centers.

L'archive ouverte pluridisciplinaire **HAL**, est destinée au dépôt et à la diffusion de documents scientifiques de niveau recherche, publiés ou non, émanant des établissements d'enseignement et de recherche français ou étrangers, des laboratoires publics ou privés.

**Comprehensive Study of the Low-Temperature Transport and Thermodynamic  
Properties of the Cluster Compounds  $\text{Ag}_x\text{Mo}_9\text{Se}_{11}$  ( $3.41 \leq x \leq 3.78$ )**

T. Zhou<sup>1</sup>, M. Colin<sup>1</sup>, C. Candolfi<sup>1</sup>, C. Boulanger<sup>1</sup>, A. Dauscher<sup>1</sup>, E. Santava<sup>2</sup>, J. Hejtmanek<sup>2</sup>, P. Baranek<sup>3</sup>, R. Al Rahal Al Orabi<sup>4</sup>, M. Potel<sup>4</sup>, B. Fontaine<sup>4</sup>, P. Gougeon<sup>4</sup>, R. Gautier<sup>4</sup>, B. Lenoir<sup>1\*</sup>

<sup>1</sup>*Institut Jean Lamour, UMR 7198 CNRS-Université de Lorraine, Parc de Saurupt, CS 50840,  
F-54011 Nancy, France*

<sup>2</sup>*Institut of Physics, Academy of Sciences of the Czech Republic, Cukrovarnicka 10, CZ-162 53  
Praha 6, Czech Republic*

<sup>3</sup>*Electricité de France, Centre des Renardières, F-77818 Moret-sur-Loing, France*

<sup>4</sup>*Institut des Sciences Chimiques de Rennes, UMR 6226 CNRS-Université de Rennes I-Ecole  
Nationale Supérieure de Chimie de Rennes, 11 allée de Beaulieu, CS 50837, F-35708 Rennes,  
France*

\*Corresponding author: [bertrand.lenoir@univ-lorraine.fr](mailto:bertrand.lenoir@univ-lorraine.fr)

**Abstract**

We present a detailed study of the evolution of the electrical, galvanomagnetic and thermodynamic properties of polycrystalline  $\text{Ag}_x\text{Mo}_9\text{Se}_{11}$  compounds for  $3.4 \leq x \leq 3.8$  at low temperatures (2 – 350 K). In agreement with density functional theory calculations, the collected data show an overall gradual variation in the transport properties from metallic to semiconducting behavior on going from  $x = 3.4$  to  $x = 3.8$ . The results evidence subtle variations in the electronic properties with the Ag content, typified by both positive and

negative phonon-drag effects together with thermopower and Hall coefficient of opposite signs. Analysis of the data suggests that these features may be due to peculiarities of the dispersion of the valence bands in the vicinity of the chemical potential. A drastic influence of the Ag content on the thermal transport has been evidenced by a pronounced change in the temperature dependence of the specific heat below 10 K. Non-linearities in the  $C_p(T^3)$  data are correlated to the concentration of Ag atoms, an increase in  $x$  resulting in a more pronounced departure from a Debye law. The observed behavior mirrors that of ionic conductors suggesting that  $\text{Ag}_x\text{Mo}_9\text{Se}_{11}$  for  $x \geq 3.6$  might belong to this class of compounds.

## I. Introduction

Thermoelectric materials are being widely studied due to their ability to convert heat into electricity (power generation) or conversely electricity into a thermal gradient (cooling applications).<sup>1-3</sup> The thermoelectric efficiency of a material is determined by the dimensionless figure of merit  $ZT = \alpha^2 T / \rho(\kappa_l + \kappa_e) = PT / (\kappa_l + \kappa_e)$  where  $\alpha$  is the thermopower,  $T$  is the absolute temperature,  $\rho$  is the electrical resistivity,  $P = \alpha^2 / \rho$  is the power factor and  $\kappa_l$  and  $\kappa_e$  are the lattice and electronic thermal conductivities, respectively.<sup>3</sup> High thermoelectric efficiency thus requires a combination of low thermal conductivity and electrical resistivity and high thermopower. These three transport parameters are however mutually interdependent and the optimization of one of them without influencing the others is extremely challenging.<sup>4</sup> One way to decouple these three quantities is to search for materials exhibiting complex crystal structure synonymous of inherently low lattice thermal conductivity values that reach the amorphous limit. This strategy then leaves the quantity  $P$  as the key factor to be adequately optimized through chemical substitutions.

Mo-based cluster compounds form several families of materials that meet this criterion. The crystal structure of these materials is composed of Mo-clusters whose nuclearity ranges from 3 ( $\text{Mo}_3$  units) up to 36 ( $\text{Mo}_{36}$  units) thereby increasing the complexity and the number of atoms per unit cell.<sup>5-7</sup> Though their transport properties were studied only scarcely so far, first experimental studies have demonstrated their poor ability to transport heat.<sup>8,9</sup> Further, the large variety of cluster's size and geometry together with the wide range of chemical compositions offer a unique playground for exploring the interplay between structural complexity and thermal transport and provide numerous possibilities to achieve high power factors.

Of the different families of Mo-cluster compounds that exist, the Chevrel phases of general formula  $M_x\text{Mo}_6X_8$  ( $M = \text{Pb, In, Ag, Cu, Fe} \dots$  with  $x$  varying from  $x = 0$  to  $x = 4$  and  $X = \text{Se, Te and S}$ ) have attracted considerable attention due to their intriguing physical properties.<sup>10-12</sup> The chemical richness of these materials enables the study of superconductivity in the presence of antiferromagnetic order in the sulphur-based compounds as well as the search for efficient thermoelectric materials in the selenium-based analogues.<sup>13-16</sup> Varying the nature and the concentration of the  $M$  atoms selectively tunes the physical properties from metallic to semiconducting behavior providing a direct method to finely optimize the power factor of these compounds. So far, the highest  $ZT$  was obtained in the double-filled  $(\text{Cu/Fe})\text{Mo}_6\text{Se}_8$  compound with  $ZT \sim 0.6$  at 1150 K.<sup>16</sup>

Recently, other Mo-based cluster compounds, namely  $\text{Ag}_3\text{In}_2\text{Mo}_{15}\text{Se}_{19}$  and  $\text{Ag}_x\text{Mo}_9\text{Se}_{11}$  ( $3.4 \leq x \leq 3.9$ ), were shown to display interesting thermoelectric properties at high temperatures with  $ZT$  values reaching 0.45 and 0.65 at 1100 and 800 K, respectively.<sup>8,9</sup> The crystal structures of these materials, built upon  $\text{Mo}_6$  and  $\text{Mo}_9$  cluster units, show high structural disorder in addition to possible dynamical degrees of freedom such as loosely bounded atoms in cage-like environments or in empty channels between the cluster units. As a result, both families of compounds exhibit very low thermal conductivity values close to the amorphous limit *i.e.* in a

regime where the phonon mean free path is of the order of interatomic distances. While the former exhibits metallic-like properties, the transport properties in the latter were shown to drastically depend on the Ag content. With increasing  $x$ , the metallic properties ( $x = 3.4$ ) smoothly evolve towards a heavily-doped semiconducting state ( $x = 3.9$ ).

The development of suitable strategies for further optimizing the thermoelectric efficiency of the  $\text{Ag}_x\text{Mo}_9\text{Se}_{11}$  compounds rests upon a better understanding of the low-temperature electronic properties and their variations with  $x$ . To address these as-yet-unexplored issues, we provide a detailed combined theoretical and experimental study of the low-temperature electrical, galvanomagnetic and thermodynamic properties of the  $\text{Ag}_x\text{Mo}_9\text{Se}_{11}$  system for  $3.4 \leq x \leq 3.8$  and partial results obtained on a nearly Ag-free sample  $\text{Ag}_{0.05}\text{Mo}_9\text{Se}_{11}$ . The experimental findings are complemented by electronic band structure calculations performed for the compositions  $x = 3.0$  and  $4.0$  including the energy dependence of the density of states and the dispersion curves. The paper is organized as follows. After presenting the key crystallographic features of these compounds along with the chemical and structural characterizations carried out, we describe the electronic band structure calculations performed with the aim of determining the evolution of the band structure as a function of  $x$ . The subsequent section is dedicated to the analysis of the specific heat data, comparing the variation of the density of states at the Fermi level with  $x$  with that derived theoretically. Finally, we discuss the temperature dependence of the thermopower followed by the electrical resistivity and Hall effect data.

## II. Experimental and computational details

**Synthesis.** Polycrystalline  $\text{Ag}_x\text{Mo}_9\text{Se}_{11}$  samples with nominal compositions  $x = 3.4, 3.5, 3.75, 3.8, 3.9$  and  $4.0$  were prepared by a two-step synthesis method. In a first step,  $\text{MoSe}_2$  was synthesized from Mo (99.999%, Alfa Aesar) and Se (99.999%, Alfa Aesar) powders in a sealed silica ampoule. Then, stoichiometric amounts of  $\text{MoSe}_2$ , Mo and Ag were placed in silica tubes sealed under argon atmosphere and heated at  $950^\circ\text{C}$  for 48h. The resulting ingots were ground into micron-sized powders and densified by spark plasma sintering (SPS) during 10 minutes at  $1050^\circ\text{C}$  under a uniaxial pressure of 80 MPa. The relative density of the cylindrical pellets, determined as the ratio between the measured and theoretical densities, is above 95 % for all samples.

Since the binary  $\text{Mo}_9\text{Se}_{11}$  compound is metastable under ambient conditions, it could not be obtained so far by any direct synthesis method. This sample was thus prepared from chemical deintercalation of Ag on a densified bar-shaped sample with  $x = 3.4$ . The chemical route utilized (described in Supporting Information) inevitably enhances the porosity that prevents reliable measurements of the electrical resistivity and thermal conductivity to be performed. Hence, these results will not be discussed in the present paper. The lattice parameters of the crystal structure, obtained from Rietveld refinements of powder x-ray diffraction patterns, were found to be slightly larger than those inferred from prior study on single crystals. This suggests an incomplete deintercalation of Ag in our polycrystalline sample further confirmed by chemical analyses (Supporting Information, Figure S1). A rough estimate of the residual Ag content was obtained by linearly extrapolating the lattice parameters as a function of  $x$  from 3.4 down to 0.0 leading to  $x \sim 0.05$ . Because of this very low Ag content, the results presented herein are expected to be very close from those of pure  $\text{Mo}_9\text{Se}_{11}$ .

**Powder X-ray Diffraction and Chemical Homogeneity.** Phase purity of the

$\text{Ag}_x\text{Mo}_9\text{Se}_{11}$  samples were checked by room-temperature powder x-ray diffraction (PXRD) data collected on a Bruker D8 Advance diffractometer equipped with  $\text{Cu K}\alpha_1$  radiation ( $\lambda = 1.5406$  Å). The evolution of the crystal structure was obtained by Rietveld refinements against x-ray diffraction patterns (Figures S2 and S3, Supporting Information). The chemical homogeneity of the samples was further checked by scanning electron microscopy using a Quanta FEG (FEI) microscope (Figure S4, Supporting Information).

**Electron Probe Microanalysis.** While only the nominal compositions of the  $\text{Ag}_x\text{Mo}_9\text{Se}_{11}$  compounds were known in the study published by some of us,<sup>9</sup> quantitative elemental analyses were carried out to determine the actual Ag content. These measurements were carried out with a JEOL JXA 8530F electron probe microanalyzer (EPMA) and the actual compositions were obtained by averaging 81 different spots on each specimen. As explained in detail elsewhere,<sup>18</sup> a single crystal of the Chevrel phase  $\text{AgMo}_6\text{Se}_8$  was used as standard in order to minimize the influence of absorption phenomena and to determine reliably the Ag concentration. The chemical formula was obtained by normalizing the Mo content to 9 Mo atoms per unit cell (Table I). Based on these results, the homogeneity range is found to lie between  $x = 3.41$  up to  $x = 3.78$  with no indications of vacancies on the Se sites in agreement with single-crystal data.<sup>20</sup> The EPMA results thus suggest an Ag solubility limit close to  $x = 3.8$ . Note that the single-crystal data reported by Gougeon *et al.*<sup>20</sup> did not evidence selenium excess. The deviations observed from 11 Se atoms per formula unit in the normalized chemical compositions are thus believed to only reflect experimental error in the EPMA measurements. Hereafter, we label the samples using the  $x$  values measured by EPMA (Table I).

**Physical Properties Measurements.** Thermopower and electrical resistivity were simultaneously measured with the thermal transport option of a physical property measurement system (PPMS, Quantum Design) in the 2 – 350 K temperature range. These measurements were performed on bar-shaped samples cut from the sintered ingots by a diamond wire-saw and

using copper bars attached onto the samples with conducting silver epoxy (Epotech, H20E). Specific heat measurements were conducted between 0.35 and 300 K on the  $x = 0.0$ , 3.41 and 3.78 samples by a conventional relaxation method using the He3 (0.35 – 4 K) and He4 options (2 – 300 K) of a PPMS under zero magnetic field ( $x = 0.0$ , 3.41 and 3.78). Additional data under magnetic fields of  $\mu_0 H = 1\text{T}$  and  $9\text{T}$  were collected on the  $x = 3.41$  sample. For this last sample, the electrical resistivity was measured down to 0.8 K using the He3 option with a standard four-points method. Hall effect measurements were performed by a five-probe method using the ac transport option of a PPMS by sweeping the magnetic fields between  $-5$  and  $+5\text{T}$  at fixed temperatures (5 – 300 K). To dismiss possible magnetoresistive contribution due to misalignment of the contacts, the Hall resistivity  $\rho_H$  was calculated from the antisymmetric part of the transverse electrical resistivity  $\rho_{xy}$  under magnetic field reversal following the formula

$$\rho_H = [\rho_{xy}(+\mu_0 H) - \rho_{xy}(-\mu_0 H)] / 2 .$$

**Electronic Band Structure Calculations.** Density functional theory (DFT) calculations were performed using the WIEN2k program package.<sup>19</sup> Since silver atoms partially occupy four different crystallographic sites, model compounds have been considered in the *Cmcm* space group. In  $\text{Ag}_3\text{Mo}_9\text{Se}_{11}$ , only the Ag3 and Ag4 sites were considered as occupied while the Ag2 site was added to model the  $\text{Ag}_4\text{Mo}_9\text{Se}_{11}$  compound. Cell parameters and atomic positions inferred from x-ray diffraction were used.<sup>20</sup> Noteworthy, DFT calculations carried out on the above-mentioned models with alternative Ag distributions (using the same X-ray cell parameters and Mo and Se atomic coordinates) have shown that the band structure hardly depends on the position of Ag atoms, specifically in the vicinity of the Fermi level.<sup>21</sup> Because the local density approximation (LDA) and generalized gradient approximation (GGA) exchange-correlation functionals are known to underestimate experimental band gaps, the modified Becke-Johnson (mBJ) functional proposed by Tran and Blaha were utilized.<sup>22</sup> These functionals yield band gaps with an accuracy similar to hybrid functionals or GW methods, but

are computationally less time-consuming.<sup>22</sup> A plane wave cutoff corresponding to  $R_{\text{MT}}K_{\text{max}} = 7$  was used, and the radial wave functions inside the non-overlapping muffin-tin (MT) spheres surrounding the atoms were expanded up to  $l_{\text{max}} = 12$ . The charge density was Fourier expanded up to the reciprocal vector  $G_{\text{max}} = 14 \text{ \AA}^{-1}$ . Total energy convergence was achieved with respect to the Brillouin zone (BZ) integration using a mesh of 500  $k$ -points. This generated 84  $k$ -points in the irreducible Brillouin zone (IRBZ). Electronic bands and density of states (DOS) were shifted so that the Fermi level lies at 0 eV.

### III. Results and Discussion

**Crystallographic Structure.** As mentioned above, the crystal structure of the  $\text{Ag}_x\text{Mo}_9\text{Se}_{11}$  compounds ( $x = 3.55$ ) has been described by Gougeon *et al.*<sup>20</sup> based on single-crystal x-ray diffraction measurement at 300 K. The evolution of the crystal structure of this family of compounds as a function of temperature and Ag content will be presented in detail in a forthcoming paper.<sup>18</sup> Herein, we restrict ourselves to the main features relevant to the analysis of the temperature dependences of the transport and thermodynamic properties and the DFT calculations.

The  $\text{Ag}_x\text{Mo}_9\text{Se}_{11}$  compounds crystallize in the orthorhombic space group  $Cmcm$  (No. 63) with the  $a$  and  $c$  cell parameters only slightly differing by a few per cent. The crystal structure, shown in Figure 1a, is built upon the  $\text{Mo}_9\text{Se}_{11}\text{Se}_6$  cluster unit formed by the bioctahedral  $\text{Mo}_9$  cluster that results from the condensation of two  $\text{Mo}_6\text{Se}_8$  units (Figures 1b and 1c). The three-dimensional network formed by these clusters leaves empty channels that can be easily observed on the projection of the crystal structure along the  $[100]$  direction (Figure 1d). The Ag atoms are distributed over four independent crystallographic sites, each of them being partially occupied (Figure 1a).

PXRD investigations have shown that the unit cell expands quasi-linearly with increasing  $x$  up to the solubility limit of Ag determined to be close to  $x = 3.8$  (Figure S5, Supporting Information). Refinements against these patterns revealed quasi-constant occupancy factors of the Ag1, Ag2 and Ag3 sites (Table S1, Supporting Information). An increase in  $x$  thus only affects the occupancy fraction of the Ag4 site that solely drives the unit cell volume expansion.

**Electronic Structure.** The electronic structure of Mo<sub>9</sub>-based cluster compounds has been studied using semi-empirical and first-principles approaches.<sup>23-30</sup> In most cases, the electronic structure of these compounds can be rationalized on the basis of the molecular orbital (MO) diagram of the Mo<sub>9</sub>Q<sub>11</sub> cluster ( $Q$  = chalcogen). This diagram is characterized by a large gap between Mo-Mo bonding and Mo-Mo antibonding MOs corresponding to a HOMO/LUMO gap for the Mo<sub>9</sub>Q<sub>11</sub><sup>4-</sup> anion. Therefore, assuming weak intercluster interactions in the three dimensional solid and the presence of monovalent Ag<sup>+</sup> cations in Ag <sub>$x$</sub> Mo<sub>9</sub>Se<sub>11</sub>, Ag<sub>4</sub>Mo<sub>9</sub>Se<sub>11</sub> is expected to be semiconducting.

The band structure of Ag<sub>4</sub>Mo<sub>9</sub>Se<sub>11</sub>, shown in Figure 2a, confirms this picture. For this compound, the direct band gap amounts to 0.7 eV. Using semi-empirical extended Hückel calculations, Hughbanks and Hoffmann reported that the optimal charge for the Mo<sub>9</sub>Q<sub>11</sub> unit, corresponding to the occupation of bonding and vacancy of anti-bonding levels, may be either -4 or -6 due to the presence of a nonbonding level in the middle of the gap.<sup>23</sup> It seems clear from the computed band structures that the lowest unoccupied flat bands are too high in energy to favor their electronic occupation. This result is consistent with the DFT diagrams of the isolated Mo<sub>9</sub>Se<sub>11</sub><sup>-4-</sup> anions previously reported.<sup>24</sup> Within the above-mentioned scenario, a rigid-band model would be expected to apply when the Ag content varies. This is what can be observed, at least qualitatively, since the band structure of Ag<sub>3</sub>Mo<sub>9</sub>Se<sub>11</sub> (Figure 2b) is very similar to that of Ag<sub>4</sub>Mo<sub>9</sub>Se<sub>11</sub>. More intriguing is the presence of regions where an inverted curvature is present such as in the  $\Gamma - Z$  direction. If we assume that a rigid-band evolution of

the bands with  $x$  is strictly valid here, the Fermi level ( $E_F$ ) of the  $x = 3$  compound would lie around 220 meV below that of the  $x = 4$  compound. These two Fermi levels thus delimit an energy window in which  $E_F$  moves upward on going from  $x = 3$  to  $x = 4$ . Interestingly, the electron pocket in the  $\Gamma - Z$  direction would start playing a role around approximately  $x = 3.3 - 3.4$  if we consider a linear evolution of the Fermi level with  $x$ . Depending on the intrinsic properties of electrons present in this pocket, both hole-like and electron-like contributions might be expected to show up in the transport properties of the  $\text{Ag}_x\text{Mo}_9\text{Se}_{11}$  phase for  $x \geq 3.4 - 3.5$ . As we shall see below, these contributions are indeed observed in the Hall transport.

Figure 3 shows the energy dependence of the total and atom-projected density of states (DOS). The top of the valence band is mainly due to the contribution of Mo atoms. As already mentioned for such units,<sup>5</sup> the outer metal atoms (Mo3 and Mo4, see Figure 1d) contribute more to the highest occupied bands than the inner metal atoms (Mo1 and Mo2) of the bioctahedral cluster. The contribution of Se atoms to the bands located in the vicinity of  $E_F$  is lower than that of molybdenum. Likewise Mo atoms, outer Se atoms, specifically Se3 and Se4, mainly contribute to the top of valence bands. Unlike the atoms forming the cluster units, Ag does not provide significant contribution to the valence bands near  $E_F$ . This conclusion is consistent with the assumed ionic interaction between Ag atoms and the cluster units and is further corroborated by DFT calculations carried out on the isostructural and hypothetical Ag-free compound  $\text{Mo}_9\text{Se}_{11}$  (not shown here). In the vicinity of  $E_F$ , the band structure computed for  $\text{Mo}_9\text{Se}_{11}$  is qualitatively similar to those depicted in Figures 2a and 2b.<sup>31,32</sup> The variation in the DOS values indicates a gradual shift from a semiconducting behavior ( $x = 4$ ) to a metallic state ( $x = 3$ ). This trend is consistent with transport properties measurements at high temperatures reported in a prior study and with our low-temperature data (see below).<sup>9</sup>

**Specific Heat.** In addition to tuning the system from metallic to semiconducting behavior, varying  $x$  is synonymous of a progressive filling of the Ag4 site located in cage-like

environment and between the Mo-Se clusters. Specific heat measurements are here used to shed light on the influence of the Ag<sub>4</sub> atoms on the thermal transport and to track the evolution of the density of states at the Fermi level with  $x$ .

Figure 4a shows the variations with temperature in the specific heat  $C_p$  for the illustrative  $x = 3.41$  and  $x = 3.78$  samples. Regardless of the Ag content, the  $C_p(T)$  data near 300 K are close to the Dulong-Petit limit  $C_p \approx C_v = 3NR$  where  $N$  is the number of atoms per formula unit and  $R$  is the ideal gas constant. For  $x = 0.05$ , an anomaly near 2 K is clearly visible (Figure 4b) suggestive of a superconducting state developing below this temperature. The critical temperature  $T_c$  contrasts with prior results obtained on a single crystal that revealed a  $T_c$  of  $\sim 5$  K.<sup>33</sup> The difference is likely due to the incomplete deintercalation of Ag in our polycrystalline sample.  $T_c$  shifts down to 1 K in the  $x = 3.41$  sample and rapidly disappears when applying a magnetic field (Figure 4c). The presence of a  $\lambda$ -type transition in  $C_p$  further suggests bulk superconductivity. As we shall see in the next section, another clear evidence is provided by the  $\rho(T)$  data, which drop to a zero-resistance regime around this temperature. Though a complete description of the superconducting state is beyond the scope of the present study, the electron-phonon coupling constant  $\lambda_{e-ph}$  can be estimated from the Debye temperature  $\theta_D$  by assuming a BCS-like superconducting state. Within this hypothesis, the critical temperature  $T_c$  is related to  $\lambda_{e-ph}$  by the McMillan formula

$$T_c = \frac{\theta_D}{1.45} \exp\left(-\frac{1.04(1 + \lambda_{e-ph})}{\lambda_{e-ph} - \mu^*(1 + 0.62\lambda_{e-ph})}\right) \text{ where } \mu^* \text{ is the renormalized Coulomb parameter.}^{34}$$

Taking  $\mu^* = 0.1$ , a value usually assumed in the superconducting Chevrel phases,<sup>10</sup> and  $\theta_D \approx 190$  K (see below), this formula yields  $\lambda_{e-ph} \approx 0.50$  and  $0.43$  for  $x = 0.05$  and  $3.41$ , respectively, suggesting an intermediate coupling regime.

Figure 4d presents the low-temperature  $C_p$  data plotted as  $C_p/T$  versus  $T^2$ . Within the Debye model, only long-wavelength acoustic phonons exist at very low temperatures contributing a  $T^3$  term in  $C_p$ . In the temperature range where this model is applicable (typically below  $\sim\theta_D/50$ ),  $C_p(T)$  follows the conventional Fermi-liquid relation  $C_p = \gamma T + \beta T^3$  where  $\gamma T$  and  $\beta T^3$  are the electronic and lattice specific heat, respectively. As shown in Figures 4c and 4d, this simple model holds for  $x = 0.05$  up to  $\sim 10$  K. The addition of Ag strongly reduces this temperature range, a linear behavior being only visible below  $\sim 2$  K in the  $x = 3.41$  sample. When  $x$  slightly increases to 3.61, a downward curvature in  $C_p(T)$  emerges and is even more pronounced as  $x$  further increases. Below  $\sim 1.2$  K, the  $\frac{C_p}{T}(T^2)$  data appear nevertheless linear which enables deriving the  $\gamma$  and  $\beta$  parameters. The values of  $\gamma$  and  $\beta$ , listed in Table II, are related to  $N(E_F)$  and  $\theta_D$ , respectively, via the formulae  $\gamma = 0.176N(E_F)$  and  $\theta_D = \left(\frac{12\pi^4 RN}{5\beta}\right)^{\frac{1}{3}}$ . In agreement with our first-principles calculations, an overall decrease in  $\gamma$  with  $x$  is observed reflecting the gradual shift of  $E_F$  towards the top of the valence bands. The non-monotonic behavior of  $\gamma$  with  $x$  suggests that a rigid-band approximation is not fully applicable in the present case. More intriguing is the fact that the Debye temperature of  $\text{Ag}_{0.05}\text{Mo}_9\text{Se}_{11}$  ( $\sim 190$  K), which is only slightly modified upon introducing Ag up to  $x = 3.53$ , suddenly drops to  $\sim 100$  K at  $x = 3.61$ . This very low value is then systematically observed for compositions in the range  $3.61 \leq x \leq 3.78$ .

Both the downward curvature and the very low  $\theta_D$  values are reminiscent to those observed in several Ag-containing ionic conductors.<sup>35,36</sup> In *e.g.*  $\text{Ag}_3\text{CuS}_2$  or  $\text{AgCuS}$ ,<sup>37,38</sup>  $C_p(T)$  shows a strong departure from a Debye behavior at low temperatures that originates from the presence of low-energy phonon modes. The Debye temperatures derived in these compounds

are typically extremely low ( $\sim 100$  K). These features are strikingly similar to those observed in the  $\text{Ag}_x\text{Mo}_9\text{Se}_{11}$  phase suggesting that the present samples may as well harbor ionic conduction. The presence of channels formed by the  $\text{Mo}_9\text{Se}_{11}$  framework together with the unusually large thermal ellipsoids of the Ag4 atoms might be considered as evidences lending credence to this picture. In any case, the clear correlation between the fractional occupancy on the Ag4 site and the low-temperature dependence of  $C_p$  shows that these atoms play a key role in determining the thermal transport in this system.

To further explore this scenario, we tried to subtract the electronic and phonon contributions from the  $C_p$  data to reveal possible additional contributions. Yet, if the  $\beta$  parameter inferred from the low-temperature data is merely used, the result of this subtraction is negative owing to the downward curvature of  $C_p(T)$ . This result thus suggests that the value of  $\beta$  is overestimated and questions the validity of the Debye model in the temperature range covered to derive this parameter. A straightforward explanation could be that the intrinsic acoustic phonon contribution is observable only at temperatures below 0.4 K. We note that an onset of a temperature change in  $C_p(T)$  seems to be present at the lowest temperatures reached (see Figure 4e), though a definitive conclusion cannot be drawn based solely on these data. In this regard, measurements at lower temperatures would be helpful in determining whether or not  $C_p(T)$  is featureless below 0.4 K. If we assume that the Debye region is not yet reached between 0.5 and 1.2 K, the value of  $\theta_D$  inferred would not then reflect the intrinsic phonon contribution. It seems reasonable to posit that  $\theta_D$  should not be strongly influenced by the Ag content over the entire  $x$  range. We therefore considered a constant Debye temperature of 180 K (Figure 4e) to estimate the phonon contribution and then subtracted the corresponding  $\gamma T$  and  $\beta T^3$  terms from  $C_p$ . The resulting data, plotted in Figure 4f as  $(C_p - \gamma T - \beta T^3)/T^3$  versus  $T$ , reveal excess specific heat, the magnitude of which strongly increases with  $x$ . While the  $x =$

3.53 sample shows a weak and broad maximum centered near 8 K, a peaked feature is discernable in the  $x = 3.61$  and  $x = 3.71$  samples to become eventually well defined for  $x = 3.78$ . The extremely low peak temperature together with the evolution of the magnitude with  $x$  is in line with results obtained in ionic conductors.<sup>35</sup> Further investigations are required to determine whether an ionic state sets in in this phase. In addition, inelastic neutron scattering experiments may unveil possible low-energy phonon modes as observed in ionic conductors such as  $\text{Cu}_{2-x}\text{Se}$  or  $\text{AgCuS}$ .<sup>38-40</sup>

**Transport properties.** Figure 5 presents the temperature dependence of the thermopower for the various Ag-filled samples and the  $\text{Ag}_{0.05}\text{Mo}_9\text{Se}_{11}$  compound. In  $\text{Ag}_{0.05}\text{Mo}_9\text{Se}_{11}$ ,  $\alpha$  shows a pronounced hump near 20 K most likely related to phonon-drag phenomenon. Above this temperature, the low  $\alpha$  values are practically temperature-independent up to 300 K and consistent with the metallic state of this compound. Our calculations have predicted that this metallic ground state remains unaffected up to  $x \leq 3.5$  before evolving towards a semiconducting state expected to develop at  $x = 4.0$ . The overall variation in the  $\alpha$  values with  $x$  is in agreement with this picture, the magnitude of  $\alpha$  increasing as  $x$  approaches the  $x = 3.78$  concentration.

For  $x < 3.71$ , the  $\alpha(T)$  data show a pronounced minimum below 70 K. The magnitude of this maximum (in absolute value) decreases upon increasing  $x$  to become positive above  $x = 3.71$  and eventually to increase with  $x$  up to  $x = 3.78$ . Nonlinearities in the thermopower are usually related to phonon-drag effect that is superimposed to the diffusion term. In the present case, the sensitivity of this peak to the Ag content is reminiscent to the Chevrel phase  $\text{Cu}_{1.8}\text{Mo}_6\text{S}_{8-y}\text{Se}_y$  where both the size of the peak and its sign evolve with  $y$ .<sup>41</sup> This evolution was shown to originate from the competition between phonon-drag and electron-phonon enhancement of the thermopower. At low Se concentrations, the former is responsible for the negative peak seen in the  $\alpha(T)$  data. As  $y$  increases, the enhanced disorder in the unit cell

results in a reduction in momentum transferred to the electrons thereby decreasing the magnitude of the phonon-drag effect. While at higher Se contents a pure diffusive regime would be then expected, a positive deviation from linearity was observed and was shown to represent a first clear example of the electron-phonon-enhancement mechanism in crystalline solids.<sup>41,42</sup> Because of the similarities between these two families of compounds, it is tempting to conclude that this last mechanism is also at play in the  $\text{Ag}_x\text{Mo}_9\text{Se}_{11}$  phase. To disentangle these two phenomena, we tried to describe the low-temperature region of the  $\alpha(T)$  curves within the model developed by Kaiser (for details of the model and the fitting procedure, see Supporting Information).<sup>43-45</sup> However, this model could not reproduce well the observed  $\alpha(T)$  data suggesting that the low-temperature peaks rather originate solely from a phonon-drag effect. This phenomenon depends on the lattice specific heat and the ratio between the electron-phonon relaxation time and the phonon relaxation time due to all other phonon scattering events.<sup>46</sup> At sufficiently low temperatures, the latter overwhelms the former so that the phonon-drag contribution is proportional to  $T^3$ . As the temperature increases, the electron-phonon relaxation time becomes larger and the phonon-drag contribution then decreases as  $T^{-1}$ . The  $\alpha(T)$  data seems to follow these trends, notably the steeper decrease around 75 K. What is most surprising, however, is that the phonon-drag evolves from negative to positive and increases in magnitude with  $x$ . In fact, the change of sign may result from variations in the balance between the normal and Umklapp phonon-electron scattering events, themselves related to details of the Fermi surface.<sup>46</sup> These two processes, which are known to lead to phonon-drag thermopowers of opposite sign (negative and positive for normal and Umklapp scattering, respectively), may result here in either a positive or negative peak depending on the Ag content.

The second feature observed – an increase in the magnitude of the positive phonon-drag peak with  $x$  – might originate from the proximity to a semiconducting state since in

semiconductors, only long-wavelength phonons interact with conduction electrons at all temperatures.<sup>47</sup> This possibility seems consistent with the specific heat data revealing the presence of low-energy phonon modes responsible for the strong deviation from linearity at low temperatures. The non-linearity observed is even more pronounced than the Ag concentration increases *i.e.* than the system approaches a semiconducting state.

Figures 6a and 6b show the temperature dependence of the electrical resistivity of the Ag-filled compounds. The  $x = 3.41$  sample shows a metallic-like behavior in agreement with band structure calculations. The sudden drop of  $\rho$  down to zero around 1 K (Figure S7, Supporting Information) further confirms the superconducting transition seen in  $C_p$ . Above  $x \geq 3.71$ , the metallic character remains down to 125 K where a steep rise in the  $\rho$  values with further decreasing temperature occurs. The fact that these samples behave as highly-doped semiconductors may explain this variation. Though a small change in the slope of  $\rho(T)$  is distinguishable near 125 K in the  $x = 3.41$  sample, a metallic-like behavior is preserved below this temperature.

A comparison of the magnetic field dependence of the Hall resistivity  $\rho_H$  at selected temperatures is shown in Figures 7a and 7b for two samples that illustrate both behaviors ( $x = 3.53$  and  $x = 3.78$ ). For  $x = 3.53$ , the  $\rho_H(\mu_0 H)$  data show a non-linear variation at 5 K (Figure 7a). The negative slope prevailing at low fields turns into a positive one above  $\mu_0 H \sim 1.8$ T indicating the coexistence of an electron-like and a hole-like signal. This and the positive sign of  $\alpha(T)$  suggest the presence of high-mobility electrons dominating the low-field region while holes, as the majority carriers, govern the high-field data. The characteristic field at which the changeover occurs increases from 1.8T at 5 K to 5T at 100 K and shows that the influence of electrons is of increasing importance with temperature. At 300 K,  $\rho_H(\mu_0 H)$  exhibits a linear behavior and an electronlike signal is solely observed (Figure 7a). This electronlike signal is no

longer influenced by varying  $x$  between 3.54 and 3.78 and is preserved over the whole temperature range measured. Yet, while the  $\rho_H(\mu_0 H)$  data are practically temperature-independent for  $x \leq 3.53$ , an evolution with  $T$ , visible for all samples in the range  $3.53 \leq x \leq 3.78$ , is clearly observed in the  $x = 3.78$  sample (Figure 7b).

Within a single-band model, the slope of the  $\rho_H(\mu_0 H)$  curves is related to the Hall coefficient  $R_H$  in the limit of zero magnetic field *i.e.*  $R_H = \left. \frac{\partial \rho_H(\mu_0 H)}{\partial (\mu_0 H)} \right|_{\mu_0 H \rightarrow 0}$ . Figure 8 shows the  $R_H(T)$  dependences for some illustrative samples. Two distinct behaviors can be distinguished. Below  $x = 3.53$ ,  $R_H$  remains essentially negative, positive values being reached only at low temperatures for  $x = 3.41$ . For this last sample, the magnitude of the signal is very low suggesting a compensation of the hole and electron contributions. Above  $x = 3.53$ , the negative  $R_H$  values are quasi-constant down to 130 K from which a strong increase (in absolute value) occurs. This trend faithfully reflects the  $\rho(T)$  data since the metallic-like dependences observed for  $x \leq 3.53$  show a steep increase below 130 K for  $x \geq 3.71$ . If we adopt a single-band scenario, this increase corresponds to a decrease in the carrier concentration following the relation  $n = -1/R_H e$ . This formula yields an electron concentration ranging between  $7.7 \times 10^{20}$  and  $1.9 \times 10^{20} \text{ cm}^{-3}$  at 300 K on going from  $x = 3.53$  to  $x = 3.78$ . However, the fact that the  $\rho_H(\mu_0 H)$  data feature both electron-like and hole-like signals and the opposite signs of  $\alpha$  and  $R_H$  suggest a multiband nature of the electrical conduction in the  $\text{Ag}_x\text{Mo}_9\text{Se}_{11}$  compounds. The above-mentioned electron concentrations then stand for upper limits of the actual carrier concentrations.

The change in the type of dominating charge carriers as a function of temperature and/or Ag content may have several origins related either to the microstructure of the samples or to peculiarities of the electronic band structure. A first possibility may be related to the presence of secondary phases giving rise to an electron-like signal in the Hall resistivity.<sup>48,49</sup> Our

chemical analyses did not evidence such phases, which seems in any case inconsistent with high-mobility electrons. A second possibility has been unveiled by our first-principles calculations showing regions of inverted curvature (also called “necks” in literature) in the  $\Gamma - Z$  direction of the Brillouin zone that nears the Fermi level. Because of this particular topology of the band structure, the charge carriers in these regions will behave as electrons under an electric or thermal gradient. The subtle influence of these necks is at the core of the opposite signs of thermopower and Hall data observed in transition metals such as Cu and also explains the development of electronlike features in the transport properties of PbTe – PbS alloys.<sup>50</sup> In the latter case, high-mobility electrons show up only at high temperatures *i.e.* when the Fermi level lies within few  $k_B T$  from the regions of positive curvature.

In the  $\text{Ag}_x\text{Mo}_9\text{Se}_{11}$  compounds, this scenario seems to enable explaining both the  $x$ - and  $T$ -dependence of the  $\rho_H(\mu_0 H)$  data. The variations in the transport properties show that the system evolves towards a semiconducting behavior with increasing  $x$ . This evolution was captured by our first-principles calculations demonstrating a shift of  $E_F$  towards the valence band edge. At low  $x$  values and at low temperatures,  $E_F$  is deep inside the valence bands so that the influence of the electron pockets is small and a hole-like signal is observed. When increasing  $x$ ,  $E_F$  moves closer to the band gap thereby increasing the concentration of electrons which eventually dominates the  $\rho_H(\mu_0 H)$  data for  $x \geq 3.54$  at all temperatures. Likewise in the PbTe – PbS alloys,<sup>50</sup> electrons start playing a role in the transport properties only when the thermal energy is high enough. This may explain why an electron-like signal is observed only above 200 K in the  $x = 3.41$  sample.

## IV. Summary and conclusion

We reported a detailed investigation of the evolution of the low-temperature transport properties of the cluster compounds  $\text{Ag}_x\text{Mo}_9\text{Se}_{11}$  for  $3.41 \leq x \leq 3.78$ . DFT calculations demonstrated that the electronic structure of the  $\text{Ag}_x\text{Mo}_9\text{Se}_{11}$  phase may be deduced from that of the isolated  $\text{Mo}_9\text{Se}_{11}$  cluster. In agreement with these first-principles calculations, increasing the Ag content drives the system towards a semiconducting regime expected to develop for  $x = 4.0$ . Our measurements revealed complex variations in the electrical properties with  $x$  featuring both positive and negative phonon drag contributions to  $\alpha$  and an intrinsic negative Hall coefficient of opposite sign with  $\alpha$ . The low dispersive degree of the band structure near the Fermi level leads to the presence of regions of positive curvature yielding an additional electron-like contribution that dominates the Hall resistivity above  $x = 3.41$ . Specific heat data indicated a pronounced change in the thermal transport upon introducing Ag in the crystal structure. This was straightforwardly captured in the low-temperature data demonstrating that non-linear behavior emerges when  $x \geq 3.61$ . The strong similarities between the  $\text{Ag}_x\text{Mo}_9\text{Se}_{11}$  compounds and ionic conductors suggest that diffusion of the Ag4 atoms through the channels of the crystal structure might occur. This and the fact that low thermal conductivity values were measured at high temperatures further suggests a close interplay between these two characteristics. A better understanding in the thermal transport in these compounds should nevertheless await for further dedicated experiments aiming at determining the role played by the Ag4 atoms on the phonon spectrum of  $\text{Mo}_9\text{Se}_{11}$ . Taken as a whole, the electrical and galvanomagnetic properties show that optimization of the thermoelectric properties requires either to reach a pure semiconducting behavior or to engineer the band structure near the Fermi level to increase its dispersive character, thereby lowering the electron-like contribution. Indeed, the presence of competing electron-like and hole-like signals inevitably limits the

magnitude of  $\alpha$ . This second strategy may be realized through substitutions on the Mo and/or Se sites since in several Mo-based cluster compounds, the main features of the band structure are dictated by the cluster unit itself, the intercluster interactions playing a minor role.

**Supporting Information Available.** Details about the synthesis of the nearly free Ag sample  $\text{Mo}_9\text{Se}_{11}$ . X-ray diffraction data and chemical characterizations of the chemical homogeneity of the samples. Description of the trends in the crystal structure upon varying the Ag content. Fitting procedure of the electron enhancement mechanism. Superconducting transition observed in the electrical resistivity data of the  $x = 3.41$  sample. This information is available free of charge via the Internet at <http://pubs.acs.org/>.

### Acknowledgements

T. Z. acknowledges the Region Lorraine for financial support. M. C. acknowledges C. Sempronichnig and the European Space Agency for financial support under NPI contract. Support from the Hubert Curien bi-lateral French-Czech Barrande project is also acknowledged. J.H. acknowledge the technical aide of MLTL (see: <http://mltl.eu>), which is supported within the program of Czech Research Infrastructures (project no. LM2011025).

## References

- <sup>1</sup> *Thermoelectrics Handbook, Macro to Nano*, edited by Rowe, D. M. (CRC Press, Taylor & Francis Group, Boca Raton FL, 2006).
- <sup>2</sup> *Thermoelectrics and its Energy Harvesting*, edited by Rowe, D. M. (CRC Press, 2012).
- <sup>3</sup> Goldsmid, H. J. in *Thermoelectric Refrigeration* (Temple Press Books, Ltd.: London, 1964).
- <sup>4</sup> Snyder, G. J.; Toberer, E. S. *Nature Mater.* **2008**, *7*, 105.
- <sup>5</sup> Gougeon, P.; Potel, M.; Gautier, R. *Inorg. Chem.* **2004**, *43*, 1257 and references therein.
- <sup>6</sup> Picard, S.; Gougeon, P.; Potel, M. *Acta Crystallogr.* **1997**, *C53*, 1519.
- <sup>7</sup> Picard, S.; Gougeon, P.; Potel, M.; *Angew. Chem.* **1999**, *38*, 2034.
- <sup>8</sup> Gougeon, P.; Gall, P.; Al Rahal Al Orabi, R.; Fontaine, B.; Gautier, R.; Potel, M.; Zhou, T.; Lenoir, B.; Colin, M.; Candolfi, C.; Dauscher, A. *Chem. Mater.* **2012**, *24*, 2899.
- <sup>9</sup> Zhou, T.; Lenoir, B.; Colin, M.; Dauscher, A.; Al Rahal Al Orabi, R.; Gougeon, P.; Potel, M.; Guilmeau, E. *Appl. Phys. Lett.* **2011**, *98*, 162106.
- <sup>10</sup> Fischer, Ø. *Appl. Phys.* **1978**, *16*, 1.
- <sup>11</sup> Lachal, B.; Junod, A.; Muller, J. *J. Low Temp. Phys.* **1984**, *55*, 195.
- <sup>12</sup> Chevrel, R.; Hirrien, M.; Sergent, M. *Polyhedron* **1986**, *5*, 87.
- <sup>13</sup> Petrovic, A.; Lortz, R.; Santi, G.; Berthod, C.; Dubois, C.; Decroux, M.; Demuer, A.; Antunes, A. B.; Paré, A.; Salloum, D.; Gougeon, P.; Potel, M.; Fischer, Ø. *Phys. Rev. Lett.* **2011**, *106*, 017003.
- <sup>14</sup> Caillat, T.; Fleurial, J. P. *J. Phys. Chem. Solids* **1998**, *59*, 1139.
- <sup>15</sup> Shi, X.; Wang, L.; Chen, L.; Chen, X. *Trans. Nonferrous Met. Soc. China* **2009**, *19*, 642.
- <sup>16</sup> Caillat, T.; Fleurial, J. P.; Snyder, G. J. *Solid State. Sci.* **1999**, *1*, 535.
- <sup>17</sup> Boulanger, C.; Lecuire, J. M.; Gougeon, P.; Potel, M.; Sergent, M. *C. R. Acad. Sc. Paris* **1986**, *303*, 37 (1986).

- <sup>18</sup> Gougeon, P.; Gall, P.; Al Rahal Al Orabi, R.; Fontaine, B.; Gautier, R.; Potel, M.; Colin, M.; Candolfi, C.; Malaman, B.; Noire, P.; Dauscher, A.; Lenoir, B. to be published.
- <sup>19</sup> Blaha, P.; Schwarz, K.; Madsen, G. K. H.; Kvasnicka, D.; Luitz, J. revised edition WIEN2k 11.1 (Release 30.03.2011), <http://www.wien2k.at>.
- <sup>20</sup> Gougeon, P.; Padiou, J.; Le Marouille, J. Y.; Potel, M.; Sergent, M. *J. Solid State Chem.* **1984**, *51*, 218.
- <sup>21</sup> Gautier, R.; Gougeon, P.; Halet, J.-F.; Potel, M.; Saillard, J.-Y. *J. Alloys Compd.* **1997**, *262-263*, 311.
- <sup>22</sup> Tran, F.; Blaha, P. *Phys. Rev. Lett.* 2009, **102**, 226401.
- <sup>23</sup> G. K. H. Madsen and D. J. Singh, *Comp. Phys. Comm.* **175**, 67 (2006).
- <sup>24</sup> T. Hughbanks, and R. Hoffmann, *J. Am. Chem. Soc.* **105**, 115 (1983).
- <sup>25</sup> S. Picard, J.-F. Halet, P. Gougeon, and M. Potel, *Inorg. Chem.* **38**, 4422 (1999).
- <sup>26</sup> S. Picard, J.-Y. Saillard, P. Gougeon, H. Noël, and M. Potel, *J. Solid State Chem.* **155**, 417 (2000).
- <sup>27</sup> P. Gougeon, M. Potel, and R. Gautier, *Inorg. Chem.* **43**, 1257 (2004).
- <sup>28</sup> D. Salloum, R. Gautier, P. Gougeon, and M. Potel, *J. Solid State Chem.* **177**, 1672 (2004).
- <sup>29</sup> D. Salloum, P. Gougeon, M. Potel, and R. Gautier, *C.R. Chim.* **11-12**, 1743 (2005).
- <sup>30</sup> P. Gougeon, P. Gall, R. Gautier, and M. Potel, *Acta Crystallogr., Sect. C: Cryst. Struct. Commun.* **C66**, i67 (2010).
- <sup>31</sup> Al Rahal Al Orabi, R. PhD from Ecole Nationale Supérieure de Chimie de Rennes, 2013.
- <sup>32</sup> R. Al Rahal Al Orabi, B. Fontaine, P. Gall, C. Candolfi, B. Lenoir, P. Gougeon, R. Gautier, to be published.
- <sup>33</sup> P. Gougeon, M. Potel, J. Padiou, M. Sergent, C. Boulanger, J. M. Lecuire, *J. Solid State Chem.* **71**, 543 (1987).
- <sup>34</sup> McMillan, W. L. *Phys. Rev.* **1968**, *167*, 331.

- <sup>35</sup> H. v. Löhneysen, H. J. Schink, W. Arnold, H. U. Beyeler, L. Pietronero, S. Strässler, *Phys. Rev. Lett.* **46**, 1213 (1981).
- <sup>36</sup> M. R. Madison, H. G. LeDuc, L. B. Coleman, *J. Chem. Phys.* **81**, 470 (1984).
- <sup>37</sup> D. M. Trots, A. Senyshyn, D. A. Mikhailova, T. Vad, H. Fuess, *J. Phys. : Condens. Matter* **20**, 455204 (2008).
- <sup>38</sup> A. N. Skomorokhov, D. M. Trots, S. G. Ovchinnikov and H. Fuess, *J. Phys. : Condens. Matter* **19**, 186228 (2007).
- <sup>39</sup> A. N. Skomorokhov, D. M. Trots, L. L. Sashin, H. Fuess, E. L. Jadrowskii, S. G. Ovchinnikov, *Phys. Solid State* **50**, 318 (2008).
- <sup>40</sup> S. A. Danilkin, M. Yethiraj, G. J. Kearley, *J. Phys. Soc. Jpn.* **79**, Suppl. A, 25 (2010).
- <sup>41</sup> A. B. Kaiser, *Phys. Rev. B* **35**, 4677 (1987).
- <sup>42</sup> A. B. Kaiser, G. Mountjoy, *Phys. Rev. B* **43**, 6266 (1991).
- <sup>43</sup> N. E. Sluchanko, V. V. Glushkov, S. V. Demishev, M. V. Kondrin, N. A. Samarin, A. K. Savchenko, A. O. Orlov, G. L. Snider, V. V. Brazhkin, V. V. Moshchalkov, *Phys. Rev. B* **56**, 10816 (1997).
- <sup>44</sup> A. B. Kaiser, *Phys. Rev. B* **29**, 7088 (1984).
- <sup>45</sup> A. B. Kaiser, A. L. Christie, B. L. Gallagher, *Aust. J. Phys.* **39**, 909 (1986).
- <sup>46</sup> F. J. Blatt, P. A. Schroeder, C. L. Foiles, D. Greig in *Thermoelectric power of metals* (Plenum Press, 1976).
- <sup>47</sup> F. J. Blatt, *Proc. Phys. Soc.* **83**, 1065 (1964).
- <sup>48</sup> H. J. de Wit, *J. Appl. Phys.* **43**, 908 (1972).
- <sup>49</sup> R. Wolfe, J. H. Wernick, S. E. Haszko *J. Appl. Phys.* **31**, 1959 (1960).
- <sup>50</sup> C. M. Jaworski, M. D. Nielsen, H. Wang, S. N. Girard, W. Cai, W. D. Porter, M. G. Kanatzidis, J. P. Heremans, *Phys. Rev. B* **87**, 045203 (2013).

## Tables

Table I. Nominal and actual compositions measured by EPMA on the polycrystalline samples.

<i>Nominal composition</i>	<i>EPMA</i>
$\text{Ag}_{3.4}\text{Mo}_9\text{Se}_{11}$	$\text{Ag}_{3.41(13)}\text{Mo}_9\text{Se}_{11.37(08)}$
$\text{Ag}_{3.5}\text{Mo}_9\text{Se}_{11}$	$\text{Ag}_{3.53(16)}\text{Mo}_9\text{Se}_{11.24(15)}$
$\text{Ag}_{3.6}\text{Mo}_9\text{Se}_{11}$	$\text{Ag}_{3.61(10)}\text{Mo}_9\text{Se}_{11.34(11)}$
$\text{Ag}_{3.75}\text{Mo}_9\text{Se}_{11}$	$\text{Ag}_{3.54(16)}\text{Mo}_9\text{Se}_{11.39(15)}$
$\text{Ag}_{3.8}\text{Mo}_9\text{Se}_{11}$	$\text{Ag}_{3.73(14)}\text{Mo}_9\text{Se}_{11.27(15)}$
$\text{Ag}_{3.9}\text{Mo}_9\text{Se}_{11}$	$\text{Ag}_{3.71(13)}\text{Mo}_9\text{Se}_{11.24(10)}$
$\text{Ag}_{4.0}\text{Mo}_9\text{Se}_{11}$	$\text{Ag}_{3.78(17)}\text{Mo}_9\text{Se}_{11.26(13)}$

Table II. Values of the  $\gamma$  and  $\beta$  parameters inferred from low-temperature specific heat analyses. The Debye temperatures  $\theta_D$  were calculated from the  $\beta$  parameters (see text). The experimental errors are estimated to be  $\pm 1 \text{ mJ}\cdot\text{mol}^{-1}\cdot\text{K}^{-2}$  and  $\pm 1 \text{ mJ}\cdot\text{mol}^{-1}\cdot\text{K}^{-4}$  for  $\gamma$  and  $\beta$ , respectively. The error in  $\theta_D$  is estimated to be less than 5%.

$x$	$\gamma$ ( $\text{mJ}\cdot\text{mol}^{-1}\cdot\text{K}^{-2}$ )	$\beta$ ( $\text{mJ}\cdot\text{mol}^{-1}\cdot\text{K}^{-4}$ )	$\theta_D$ (K)
0.05	31	5.3	194
3.41	41	7.3	184
3.53	40	7.3	198
3.61	20	36	110
3.71	22	61	91
3.78	12	54	95

## Figure Captions

Figure 1: (a) Crystal structure of the  $\text{Ag}_x\text{Mo}_9\text{Se}_{11}$  compounds highlighting the four inequivalent crystallographic positions of the Ag atoms labeled from Ag1 to Ag4. (b) Formation of the  $\text{Mo}_9\text{Se}_{11}$  cluster by the condensation of two  $\text{Mo}_6\text{Se}_8$  units. (c)  $\text{Mo}_9\text{Se}_{11}$  cluster unit showing the four Mo and five Se positions. (d) Projection along the [100] direction of the three-dimensional network formed by the  $\text{Mo}_9\text{Se}_{11}$  clusters.

Figure 2: DFT dispersion curves of the  $\text{Ag}_4\text{Mo}_9\text{Se}_{11}$  (a) and  $\text{Ag}_3\text{Mo}_9\text{Se}_{11}$  (b) model compounds.

Figure 3: DOS of the model compound  $\text{Ag}_4\text{Mo}_9\text{Se}_{11}$ . The dotted and dashed lines indicate the Fermi level for  $x = 3$  and  $x = 4$  in  $\text{Ag}_x\text{Mo}_9\text{Se}_{11}$ , respectively.

Figure 4: (a) Specific heat  $C_p$  as a function of temperature of the  $x = 3.53$  (■) and  $x = 3.78$  (●) samples. (b) Low-temperature  $C_p$  data of  $\text{Ag}_{0.05}\text{Mo}_9\text{Se}_{11}$  displayed as  $C_p/T$  versus  $T$  to highlight the superconducting transition. (c)  $C_p/T$  as a function of  $T^2$  of the  $x = 3.41$  sample measured under a magnetic field of  $\mu_0 H = 0\text{T}$  (●),  $1\text{T}$  (■) and  $9\text{T}$  (▲). (d) Low-temperature  $C_p/T$  data plotted as a function of  $T^2$  of the  $x = 0.05$  (◆),  $x = 3.53$  (■) and  $x = 3.78$  (●) samples. (e)  $C_p/T$  versus  $T^2$  of the  $x = 3.78$  (●) sample. The solid black line passing through the data points stand for the best fit to the data according to the relation  $C_p = \gamma T + \beta T^3$ . The second solid black line exhibits a smaller slope that corresponds to a Debye temperature of 180 K. (f)  $(C_p - \gamma T - \beta T^3)/T^3$  data of the  $x = 3.41$  (●),  $x = 3.71$  (▲),  $x = 3.78$  (●) samples plotted as a function of temperature. The  $\beta$  parameter has been calculated assuming a constant Debye temperature of 180 K for all compounds.

Figure 5: (a) Temperature dependence of the thermopower  $\alpha$  of the  $\text{Ag}_x\text{Mo}_9\text{Se}_{11}$  compounds for  $x = 0.05$  ( $\diamond$ ),  $x = 3.41$  ( $\bullet$ ),  $x = 3.53$  ( $\blacksquare$ ),  $x = 3.54$  ( $\blacktriangle$ ),  $x = 3.61$  ( $\blacklozenge$ ),  $x = 3.71$  ( $\blacktriangle$ ),  $x = 3.73$  ( $\blacktriangledown$ ) and  $x = 3.78$  ( $\bullet$ ). (b) Magnification of the low-temperature data to highlight the phonon-drag contribution. The solid black line is a guide to the eye.

Figure 6: (a) Temperature dependence of the electrical resistivity  $\rho$  of the  $\text{Ag}_x\text{Mo}_9\text{Se}_{11}$  compounds for  $x = 3.41$  ( $\bullet$ ),  $x = 3.53$  ( $\blacksquare$ ),  $x = 3.54$  ( $\blacktriangle$ ),  $x = 3.61$  ( $\blacklozenge$ ),  $x = 3.71$  ( $\blacktriangle$ ),  $x = 3.73$  ( $\blacktriangledown$ ) and  $x = 3.78$  ( $\bullet$ ). (b) Plot of the  $\rho(T)$  data on a logarithmic scale to underline the change of slope below 125 K in the  $x = 3.41$  ( $\bullet$ ),  $x = 3.53$  ( $\blacksquare$ ),  $x = 3.54$  ( $\blacktriangle$ ) and  $x = 3.61$  ( $\blacklozenge$ ) samples.

Figure 7: Magnetic field dependence of the Hall resistivity  $\rho_H$  at selected temperatures of the (a)  $x = 3.53$  and (b)  $x = 3.78$  samples. In both panels, the data were collected at  $T = 5$  ( $\bullet$ ), 35 ( $\blacksquare$ ), 55 ( $\blacklozenge$ ), 100 ( $\otimes$ ), 150 ( $+$ ) and 300 K ( $\blacktriangle$ ).

Figure 8: Temperature dependence of the Hall coefficient  $R_H$  for the  $x = 3.53$  ( $\blacksquare$ ),  $x = 3.54$  ( $\blacktriangle$ ),  $x = 3.73$  ( $\blacktriangledown$ ) and  $x = 3.78$  ( $\bullet$ ) samples.

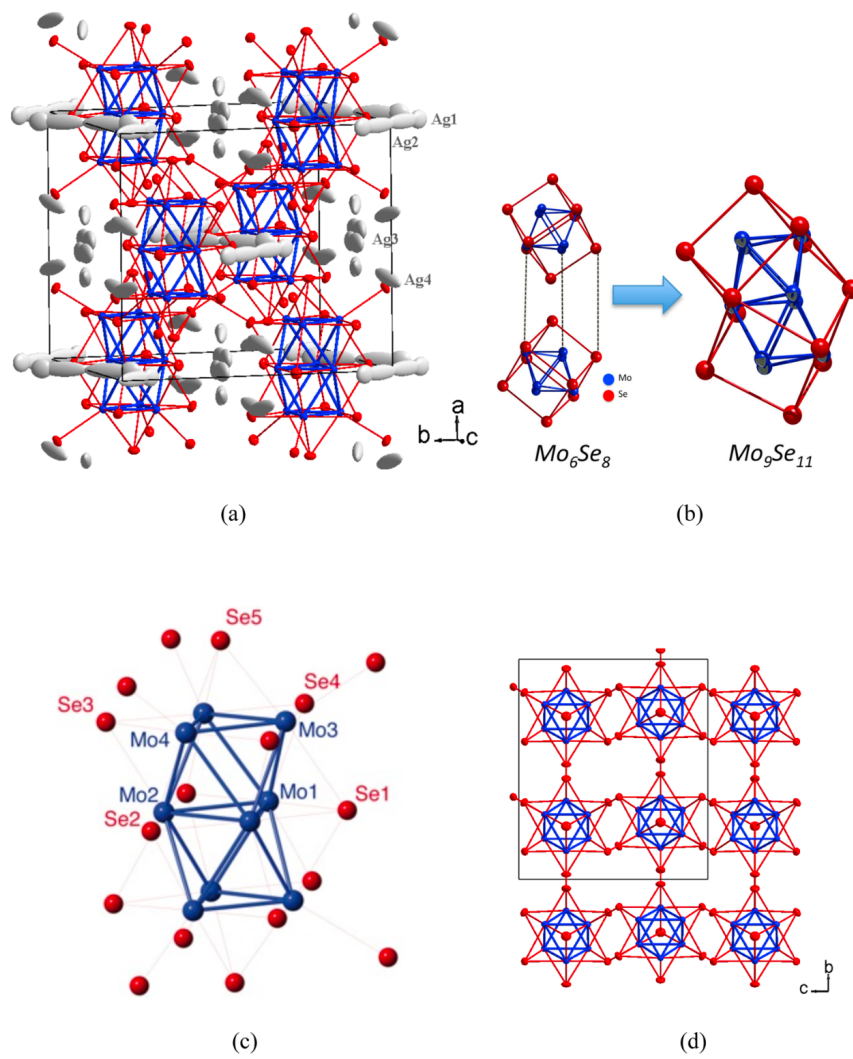


Figure 1

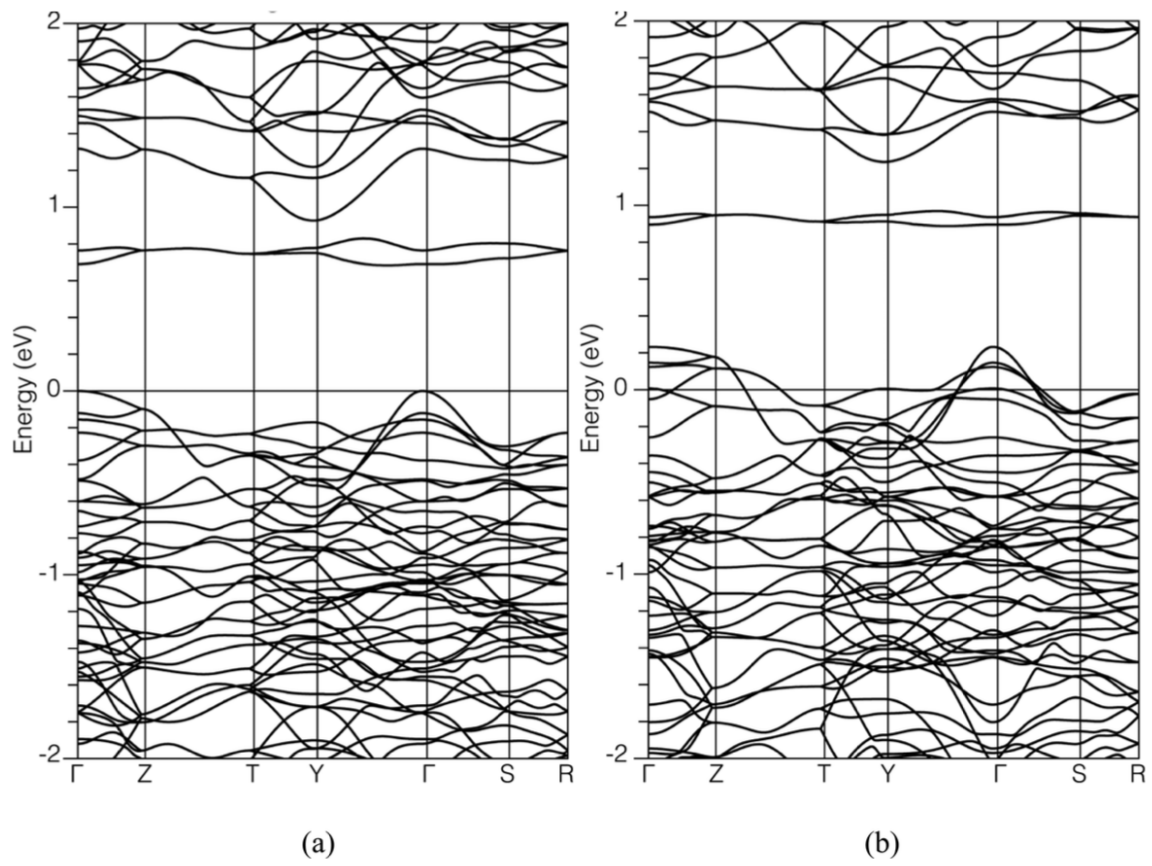


Figure 2

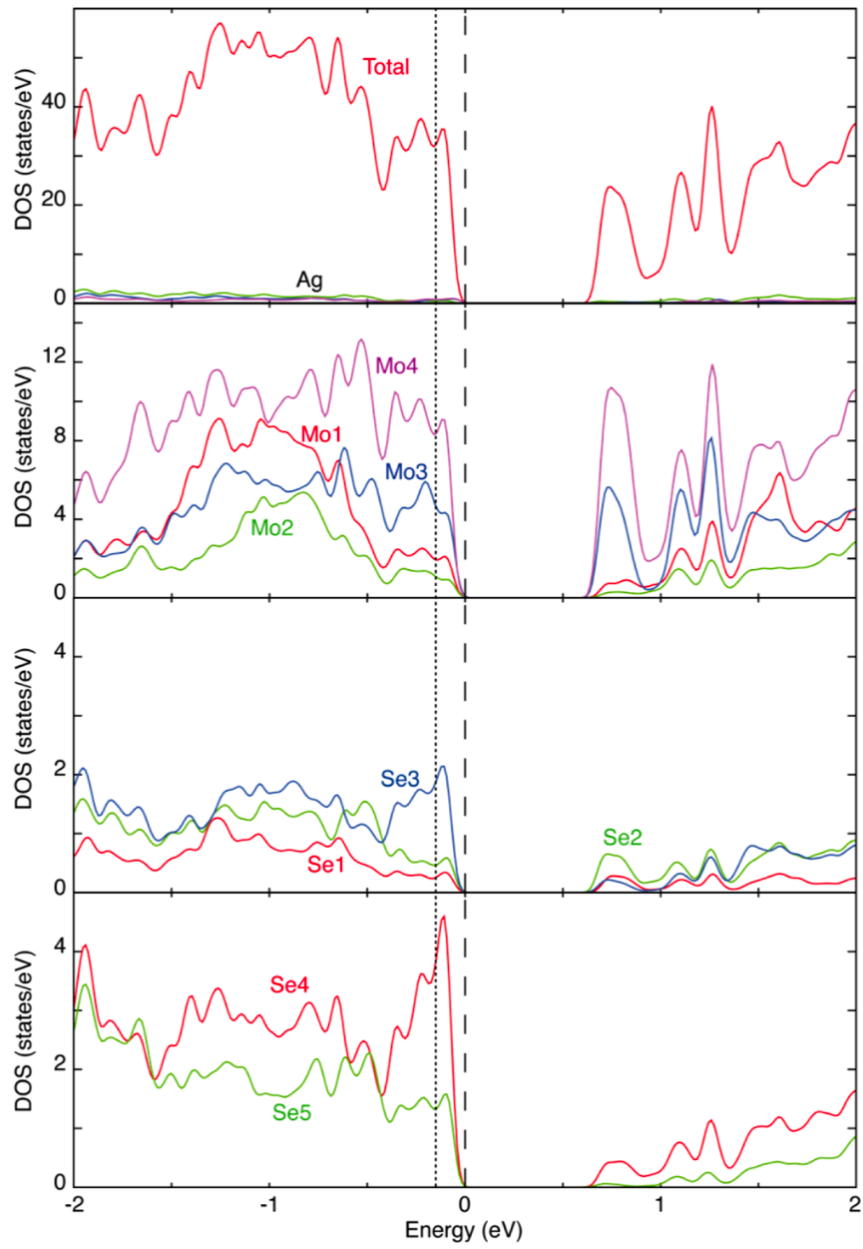


Figure 3

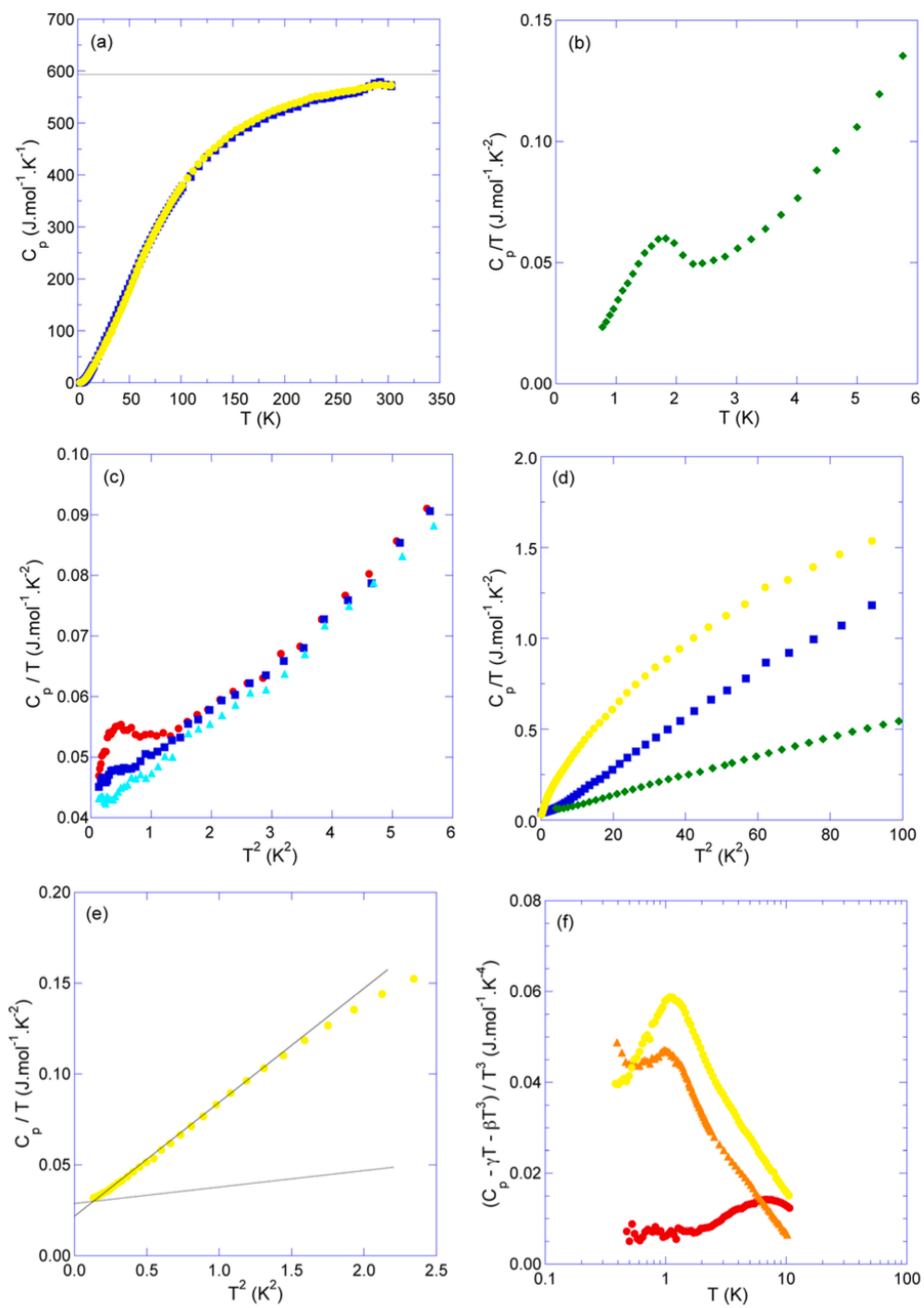


Figure 4

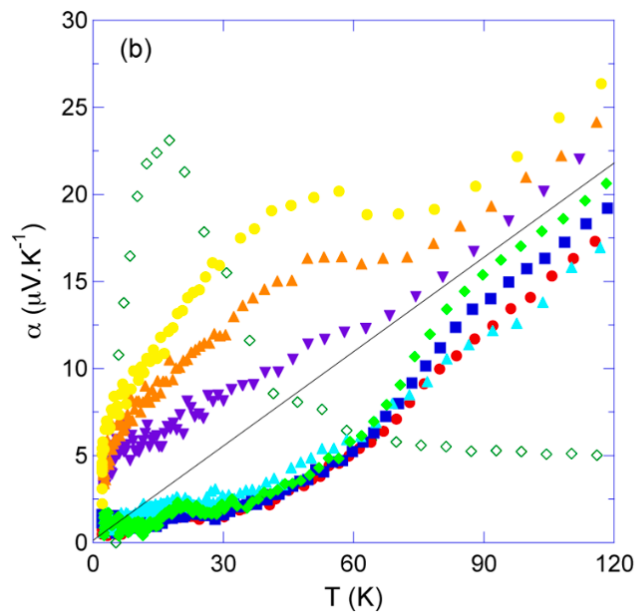
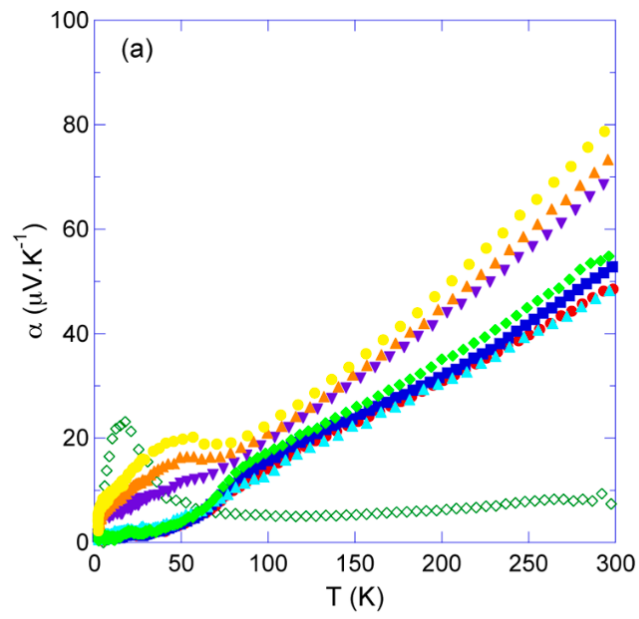


Figure 5

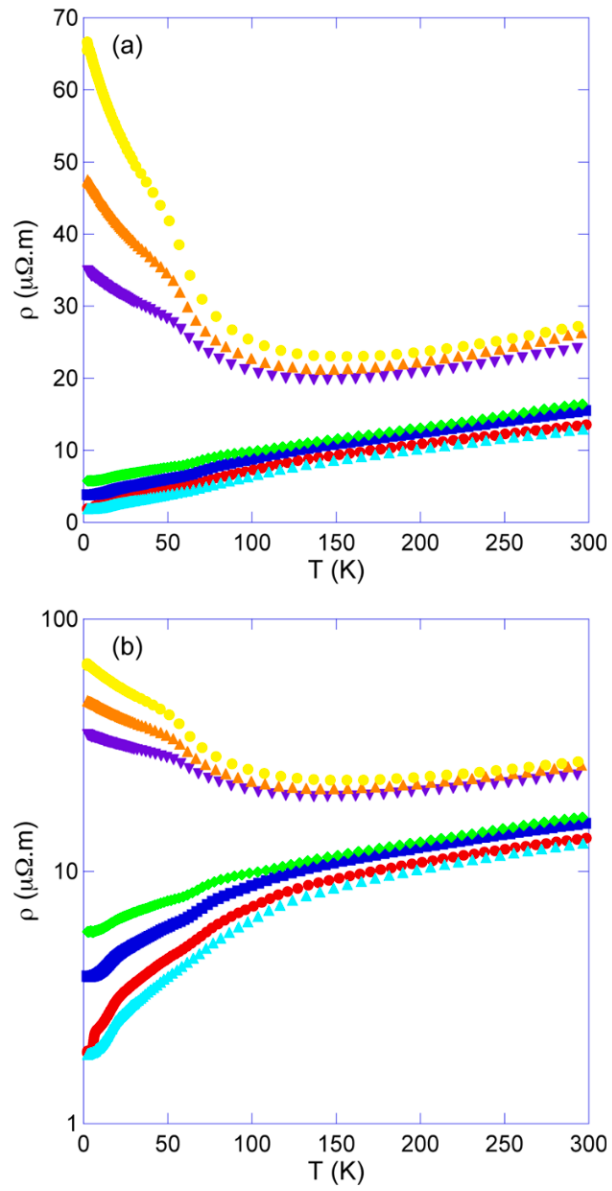


Figure 6

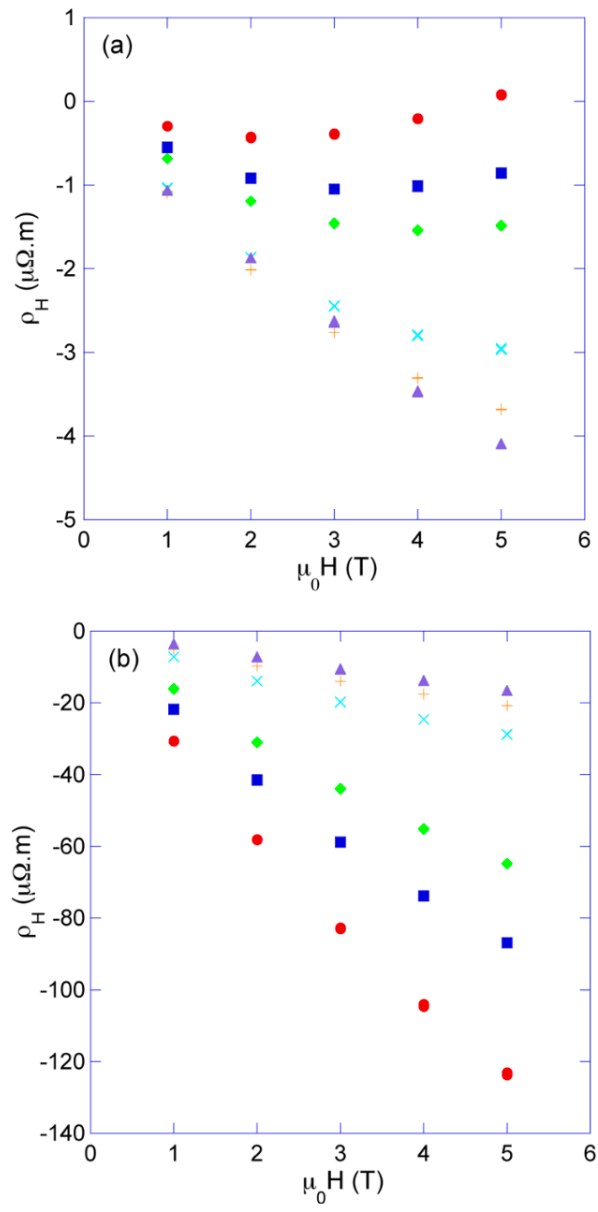


Figure 7

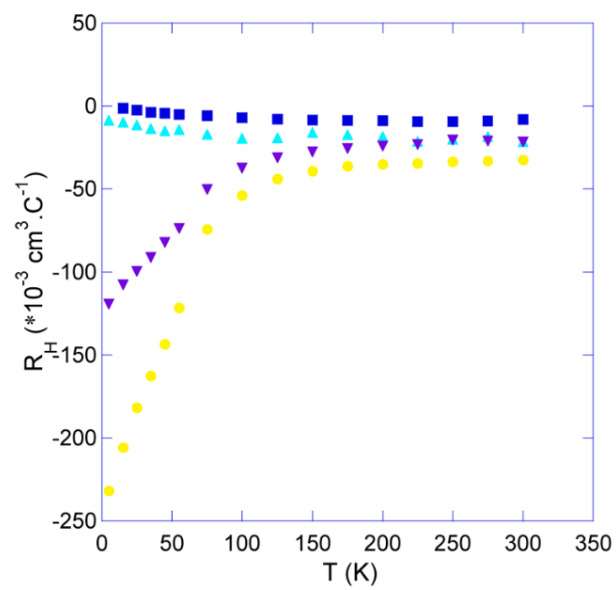


Figure 8

## Table of Contents Graphic

